Modeling SEBM process of tantalum lattices

Mingkai Yue and Meie Li
Xi'an Jiaotong University, Xi'an, China
Ning An
Sichuan University, Chengdu, China
Kun Yang and Jian Wang
Northwest Institute for Non-ferrous Metal Research, Xi'an, China, and
Jinxiong Zhou
Xi'an Jiaotong University, Xi'an, China

Abstract

Purpose – Selective electron beam melting (SEBM) is one of the popular powder-bed additive manufacturing (AM) technologies. The purpose of this paper is to develop a simulation strategy for SEBM process to get data which are vital for realistic failure prediction and process parameters control for real complex components.

Design/methodology/approach – Focusing on the SEBM process of tantalum, this paper presents a three-dimensional thermo-mechanical modeling strategy based on ABAQUS and its subroutines. The simulation strategy used in this paper is developed for SEBM process of pure tantalum but could be extended to other AM fabrication technologies and other metals without difficulties.

Findings – The simulation of multi-track multi-layer SEBM process of tantalum was carried out to predict the temperature field, the molten pool evolution and the residual stress distribution. The key information such as inter-track molten pool overlapping ratio and inter-layer refusion state can be extracted from the obtained molten pool morphologies, which are vital for realistic failure prediction and process parameters control for real components. The authors finally demonstrate the capability of the strategy used by simulating a 2 mm × 2 mm × 10 mm lattice structure with total 200 layers.

Originality/value – The simulation of multi-track multi-layer SEBM process of tantalum was carried out. The key information such as inter-track molten pool overlapping ratio and inter-layer refusion state can be extracted. The authors finally demonstrate the capability of the strategy used by simulating a lattice structure. Not only temperature distribution but also stress evolution are captured. Our simulation strategy is developed for the SEBM process of pure tantalum, but it could be extended to other AM fabrication technologies and other metals without difficulties.

Keywords Selective electron beam melting (SEBM), Additive manufacturing (AM), Multiple tracks and multiple layers simulation, Tantalum, Lattice structure, Finite element method (FEM)

Paper type Research paper

1. Introduction

Tantalum is a versatile refractory metal with diverse applications, ranging from superalloys, capacitors and electronics, to biological and medical applications. As tantalum has high melting point (approximately 2980°C) and a high propensity for oxidation, its fabrication remains a challenge. The recently emerged additive manufacturing (AM), however, provides a new solution to the issues of fabrication of tantalum. Understanding and exploring the thermal process and residual stress evolution during AM process of tantalum is crucial for failure control and process optimization. The related studies on modeling of AM of tantalum are very sparse, albeit of a few experimental efforts using either selective laser melting (SLM) (Sing *et al.*, 2018; Thijs *et al.*, 2013; Zhou *et al.*, 2017) or selective electron beam melting (SEBM) (Dong *et al.*, 2019; Choi *et al.*, 2009; Parthasarathy *et al.*, 2010; Herzog *et al.*, 2016).

Lattice structure material is composed of microstructures of periodic architectures that include micro-truss assemblies. It could be multifunctional, lightweight and easy to design (Evans *et al.*, 2001). Therefore, it has potential applications in medical implants, spacecraft parts, engine parts and so on (Beyer, 2014; Lu *et al.*, 2006; Tancogne-Dejean *et al.*, 2018; Wong and Hernandez, 2012; Queheillalt and Wadley, 2005; Rahmani *et al.*, 2019; Soro *et al.*, 2019; Dumas *et al.*, 2017; Vasiliev *et al.*, 2012). The traditional manufacturing methods of lattice materials mainly include investment casting, metallic wire braiding, metallic wire assembly, superplastic forming and extrusion (Pan *et al.*, 2020; Wang *et al.*, 2003; Wadley *et al.*, 2003). These methods have many obvious shortcomings and limits in manufacturing lattice structure. Besides,

The current issue and full text archive of this journal is available on Emerald Insight at: **https://www.emerald.com/insight/1355-2546.htm**

Rapid Prototyping Journal
29/2 (2023) 232–245
 [ISSN 1355-2546]
[DOI 10.1108/RPJ-05-2022-0152]

This research is supported by National Natural Science Foundation of China (Grant 11972277).

In the interest of transparency, data sharing and reproducibility, the author(s) of this article have made the data underlying their research openly available. It can be accessed by following the link here: https://github.com/XJTU-Zhou-group/ABAQUS-Codes-for-AM-Process-of-Tantalum.

Received 15 May 2022
Revised 4 July 2022
Accepted 4 July 2022

time-consuming and cumbersome post-processing, resulting in high energy consumption and low material utilization, is inevitable. Comparatively, AM can produce complex structure and has more adaptability and accuracy, which makes it very suitable for manufacturing lattice materials.

As one of the typical powder-bed fusion AM technologies for metallic components, SEBM is featured by low residual stress, rapid fabrication speed and high energy efficiency. In addition to vast efforts to use SEBM to fabricate various metals, including titanium, stainless steel, aluminum, Inconel 718 and tantalum, numerical simulations, mainly finite element methods (FEMs), have also been developed to model the heat transfer and residual stress development during SEBM. Zäh and Lutzmann (2010) developed the FEM method to simulate the SEBM process of stainless steel (316 L). Shen and Chou (2012) built a FEM simulation framework based on the commercial software ABAQUS to model the transient thermal process of SEBM of titanium. Cheng and Chou (2015) presented a two-dimensional thermo-mechanical coupling analysis to predict the residual distortion of a Ti6Al4V overhang structure. They also extended the simulations to SEBM and SLM processes for Ti6Al4V and In718 (Cheng *et al.*, 2014; Cheng *et al.*, 2016). Galati *et al.* (2017) programmed several subroutines to model the energy source and powder material properties for SEBM process, giving a versatile and reliable SEBM simulation tool. In line with the procedures of Cheng *et al.* (2014) and Galati *et al.* (2017), the authors (An *et al.*, 2021) described the finite element implementation of both ABAQUS user subroutines and AM Modeler plugins for thermal analysis of SEBM for Ti6Al4V. For the state-of-art study on numerical simulation of SEBM, see the review paper by Galati and Iuliano (2018). Denlinger *et al.* (2017) described a three-dimensional finite element model to predict the temperature, residual stress and distortion in multi-layer SLM process. Li *et al.* (2016, 2017) developed a multi-scale modeling approach to predict residual stress and distortion of SLM process. More recently, Yan *et al.* (2018) reported in integrated simulation environment for SEBM process of multi-track multi-layer, by merging discrete element method for powder spreading and computational fluid dynamics method for powder melting. Li *et al.* (2018) presented a thermo-mechanical model in the SLM process considering the phase transition and volume shrinkage. In addition, biological and medical applications of tantalum call for the fabrication of cellular materials. Many scholars explored the technological factors affecting the quality of some classic lattice structures made by AM (Helou and Kara, 2018; Duan *et al.*, 2020; Yuan *et al.*, 2017; Gorguluarslan *et al.*, 2016; Helou *et al.*, 2016; Xiao *et al.*, 2018; Dallago *et al.*, 2019; Leary *et al.*, 2016; Sing *et al.*, 2018; Li *et al.*, 2012; Xiao *et al.*, 2019; Warmuth *et al.*, 2016; Takezawa *et al.*, 2018; Suard *et al.*, 2015). The SEBM process of cellular materials involves complicated scanning strategies, and modeling of such a process is untouched in literature, to the best knowledge of the authors.

In this study, we model the SEBM process of multi-track and multi-layer of pure tantalum. On the basis, we model the SEBM process for lattice materials by exploiting the capability of model change and progressive element activation. The paper is organized as follows: the equations, methodologies and the parameters used in simulation are described in Section 2; Section 3 provides the results for single track SEBM of tantalum to give a better understanding of the molten pool morphologies of tantalum and its influential factors; Section 4 gives the results of multi-track and multi-layer SEBM process, with inter-track and inter-layer influences highlighted; Section 5 demonstrates the modeling of a periodic lattice structure fabricated via 200 layers of SEBM process; finally, concluding remarks and perspectives are given in Section 6.

2. Modeling

In this section, we will present the analyses that are used to investigate the temperature and thermal stress distributions in the SEBM process of multi-track multi-layer. First, we will present the temperature-dependent thermo-physical properties of both solid and powder tantalum. Then, we will focus on the sequentially coupled thermal-stress analysis which is performed by first conducting a transient heat transfer analysis for predicting the temperature distributions in the structure and then performing a stress/deformation analysis for the prediction of thermal stress and deformation fields. Finally, we will outline the implementation details of the analyses in ABAQUS package.

2.1 Material parameters

One of the key issues associating with SEBM modeling is the determination of thermo-physical properties of powders, which are quite different from that of bulk solid. If experimental data is available, then it can be used readily, but so far, the experimental measurement of powder parameters remains a challenge and the results are quite scattered. When no experimental data is available, recourse is made to some approximate theory to estimate the thermo-physical parameters of powders by using the experimentally easily measurable properties of solid materials. Here, we adopt the method by Tolochko *et al.* (2003), which was originally proposed for deriving conductivity of titanium powder from solid during laser sintering. According to the model, the effective conductivity of the powder is composed of contributions from radiation, k_r, and from contact of powder particles, k_c, but the contribution from convection is ignored in vacuum. k_r is approximated as:

$$k_r \approx \frac{16}{3} l \sigma T^3 \tag{1}$$

in which l is the mean free path which is set to the particle diameter of powders, $\sigma = 5.67 \times 10^{-8} W/(m^2 K^4)$ is the Stefan-Boltzman constant and T is temperature. The conductivity because of powder contact, k_c, is estimated as:

$$k_c = \Lambda k_{bulk} x \tag{2}$$

Here, $\Lambda = \sqrt{3}$, $x = b_{neck}/R$ is the relative size of contact necks with b_{neck} radio of contact neck and R radius of powder particle, and k_{bulk} is the conductivity of solid.

The density of powder is related to the density of solid via a simple relation by considering the porosity effect and given by:

$$\rho_{powder} = (1-p)\rho_{solid} \tag{3}$$

where $p = 0.5$ is the porosity of the powder and fixed as 0.5 in the following analyses; ρ_{powder} and ρ_{solid} are respective densities of the powder and the solid. The conductivity and the density of the powders as mentioned above are plotted in Figures 1(a) and 1(b) together with that of the solid materials. In simulation, the material state, either solid or powder, is switched according to a criterion $T > T_{melt}$ and $\frac{dT}{dt} < 0$ with $T_{melt} = 3{,}253\ K$. The specific heat of powder is taken as that of the solid, as shown in Figure 1(c). In addition, the temperature-dependent mechanical properties such as Young's modulus, yield stress and thermal expansion coefficient of the solid tantalum taken from literature (Shabalin, 2014; Powell *et al.*, 1968; Škoro *et al.*, 2011; Škoro *et al.*, 2012; Tantalum, 2021) are also given in Figures 1(d)–(f).

2.2 Thermal analysis

The thermal analysis of the SEBM process is governed by the following transient heat transfer equation:

$$k_{(T)}\nabla^2 T + Q = \rho_{(T)}c_{(T)}\frac{\partial T}{\partial t} \tag{4}$$

where T is the temperature, Q is the body heat flux and $k_{(T)}$, $\rho_{(T)}$ and $c_{(T)}$ are thermal conductivity, density and specific heat as function of temperature, respectively. In SEBM and other AM processes, the body heat flux is the contribution of a moving heat source, which is either approximated by a Gauss or Goldak distribution. For the latter, it is given as (Goldak, 1985; Fachinotti *et al.*, 2011):

$$Q(x,y,z,t) = \frac{6\sqrt{3}P\eta}{\pi\sqrt{\pi}ab}\begin{cases}\frac{f_f}{c_f}\exp\left(-3\frac{(x-x_0)^2}{c_f^2}-3\frac{(y-y_0)^2}{a^2}-3\frac{(z-z_0)^2}{b^2}\right), & x > vt\\ \frac{f_r}{c_r}\exp\left(-3\frac{(x-x_0)^2}{c_r^2}-3\frac{(y-y_0)^2}{a^2}-3\frac{(z-z_0)^2}{b^2}\right), & x < vt\end{cases} \tag{5}$$

Here, $P = UI_b$ is power of heat source, U is the applied voltage, I_b is electron beam current, η is absorptivity of the material and the four geometric parameters a, b, c_f and c_r represent the half width, the depth, the front and rear length of the double ellipsoidal heat source. In this paper, $a = 0.25mm$, $b = 0.2mm$, $c_f = c_r = 0.25mm$, $\eta = 0.8$, $f_f = 2c_f/(c_f + c_r)$, $f_r = 2c_r/(c_f + c_r)$.

The heat transfer equation, equation (4), is supplemented by boundary conditions. As shown in Figure 2(a), the powders are typically put on the top of a solid substrate, whereby the heat transfer equation is also invoked. For the bottom surface of substrate, a fixed preheating temperature, $T_{pre} = 1{,}123\ K$, was enforced during the manufacturing process, while a fixed environment temperature, T_{env}, was assumed after the completion of the part. The top and side surfaces of the system, including substrate and powders, were enforced with radiation boundary condition. The radiation condition is expressed as:

$$-k\frac{\partial T}{\partial n} = \sigma\epsilon\left(T^4 - T_{env}^4\right), \tag{6}$$

The ambient environment temperature, T_{env}, is set to the preheating temperature, during the manufacturing process and then to the room temperature upon the completion of the part. $\partial T/\partial n$ is the directional derivative of temperature along the outward normal of the surface, σ, is the Stefan–Boltzman constant; $\epsilon = 0.3$ is the emissivity of material. The transient heat transfer equation, equation (4), was solved by prescribing initial conditions with the uniform temperatures of solid and power all set to equal to preheating temperature 1,123 K.

2.3 Stress analysis

As mentioned above, the solid substrate, the printed part and the surrounding powder are all considered in heat transfer analysis. In contrast, only the substrate and the printed part are considered in stress analysis, and the surrounding powders are neglected. This assumption tremendously reduces the computational cost.

Assuming the system is in the state of static equilibrium and, furthermore, neglecting any body force such as the gravity, the governing equation of mechanical equilibrium states that:

$$\nabla \cdot \sigma = 0 \tag{7}$$

The total strain of a solid is split into three parts and expressed as:

$$\epsilon^{total} = \epsilon_{ij}^{el} + \epsilon_{ij}^{pl} + \epsilon_{ij}^{T} \tag{8}$$

where ϵ_{ij}^{el}, ϵ_{ij}^{pl} and ϵ_{ij}^{T} are elastic, plastic and thermal strains, respectively. The linear relation holds for the thermal strain:

$$\epsilon_{ij}^{T} = \alpha\Delta T\delta_{ij} \tag{9}$$

with α is the coefficient of thermal expansion. The solid was assumed to be ideal elastic plastic, and the stress state is dictated by:

$$\begin{aligned}\sigma &= E\epsilon\ , \quad when \quad \epsilon \le \epsilon_s\\ \sigma &= \sigma_s\ , \quad when \quad \epsilon > \epsilon_s\end{aligned} \tag{10}$$

where E is the Young's modulus, ϵ_s is the yield strain and σ_s is the yield stress. Plastic flow occurs when the calculated effective stress $\overline{\sigma}$ given below equals or exceeds the yield stress:

$$\overline{\sigma} = \frac{\sqrt{2}}{2}\sqrt{(\sigma_{11}-\sigma_{22})^2 + (\sigma_{22}-\sigma_{33})^2 + (\sigma_{33}-\sigma_{11})^2} \tag{11}$$

2.4 Implementation in software

The methodology is an extension of our previous simulation method for titanium (An *et al.*, 2021). User subroutines, including DFLUX for moving heat source as well as UMATHT for thermo-physical properties prescribing and switching, were programmed and validated by solving some benchmark problems. The layer-wise scanning strategy was implemented by writing an input file for ABAQUS. The powerfulness of pre- and post-processing of commercial software, in together with some specific functionalities, such as model change and progressive element activation, was exploited to develop a strategy to model SEBM process of multi-track multi-layer without interruption of running of ABAQUS. This was realized by programming Python scripts to execute these capabilities. The whole simulation domain for

Figure 1 Thermo-physical properties of solid (Shabalin, 2014; Powell *et al.*, 1968; Škoro *et al.*, 2011; Škoro *et al.*, 2012; Tantalum, 2021) and powder tantalum materials

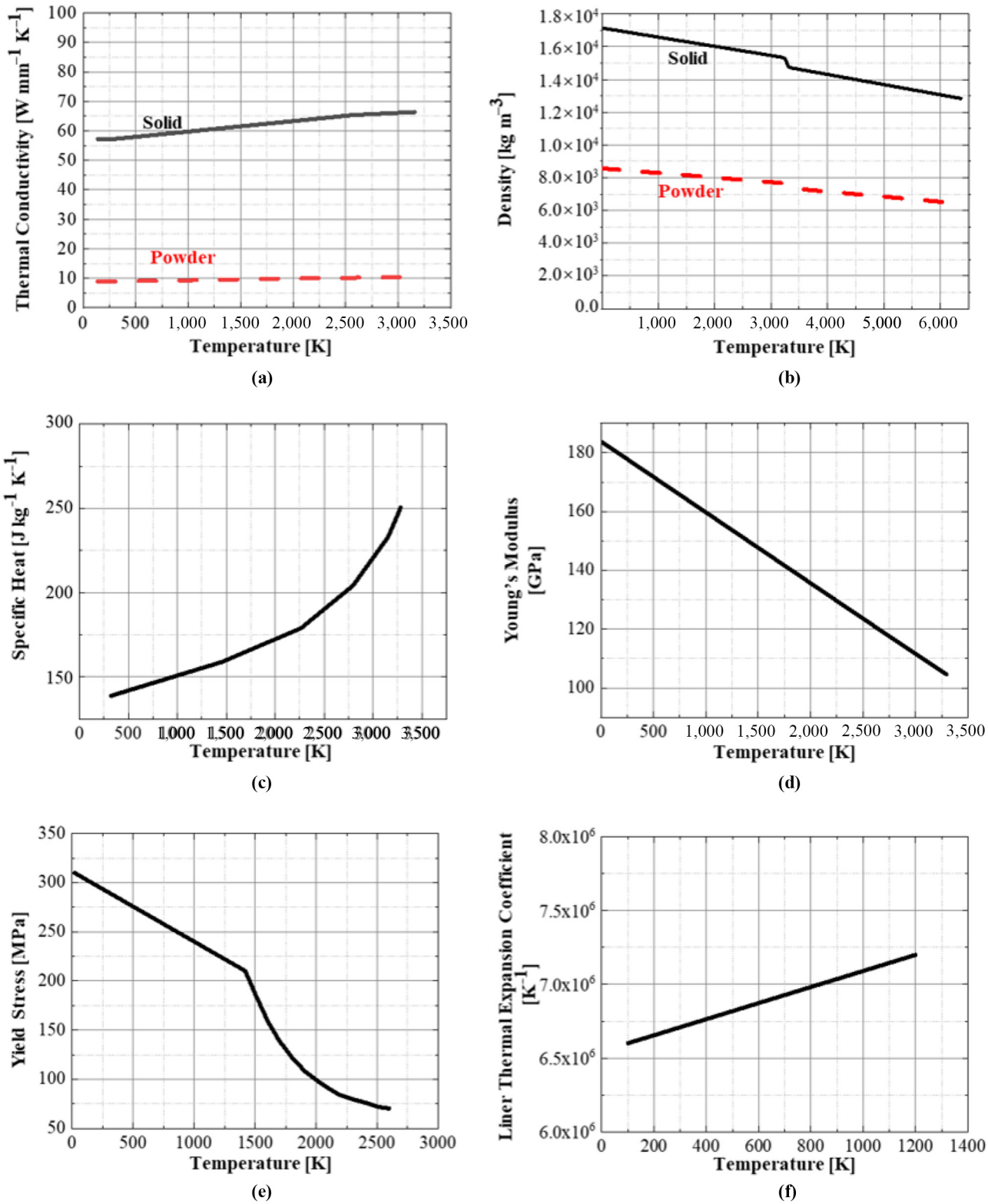

Notes: (a) Thermal conductivities of solid and powder; (b) densities of solid and powder; and (c)–(f) temperature-dependent properties of specific heat, Young's modulus, yield stress and thermal expansion coefficient of solid tantalum materials, respectively

Figure 2 Simulation of a single track scanning

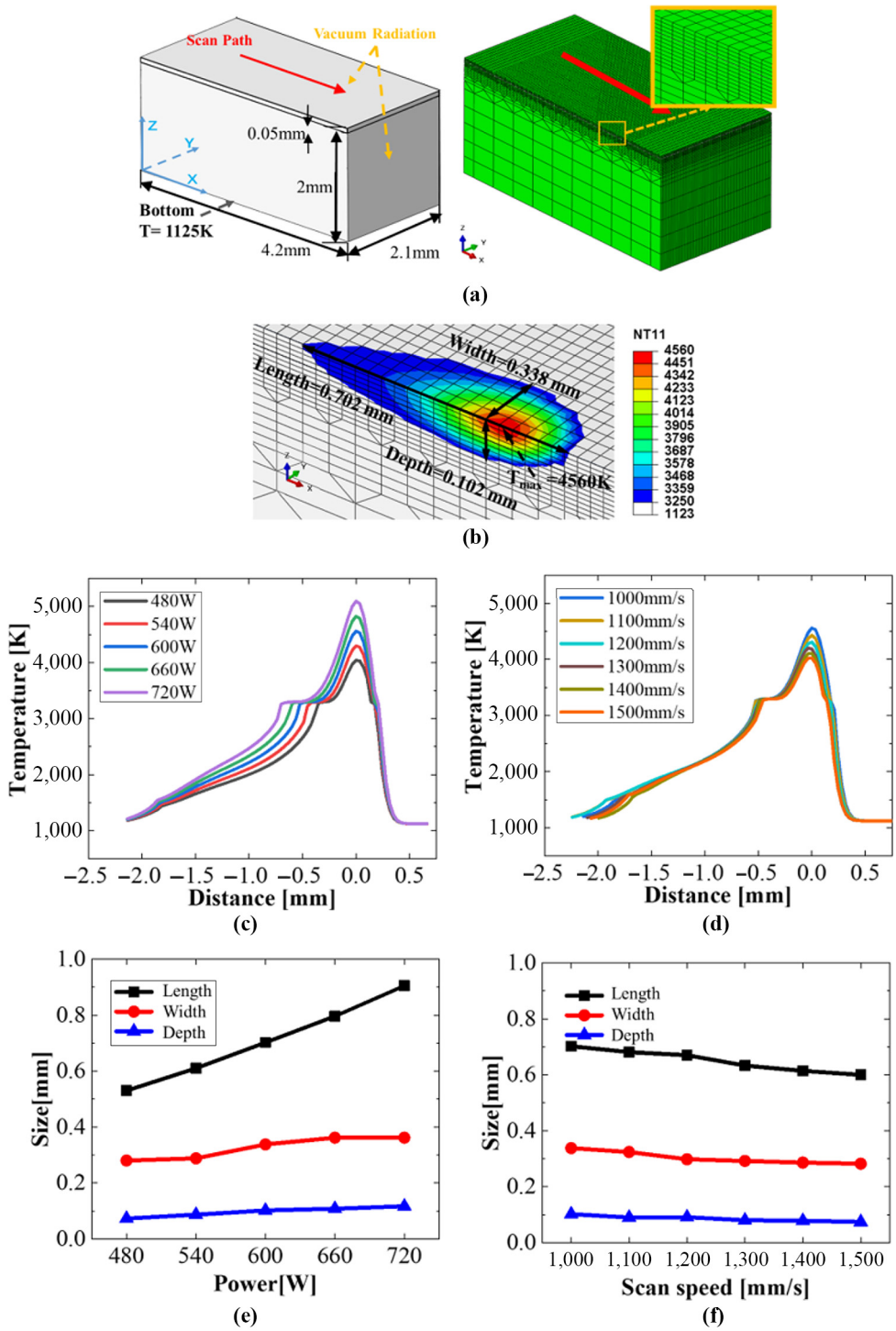

Notes: (a) Computational model and meshing; (b) predicted molten pool sizes with beam power 600 W and scan speed 1,000 mm/s; (c) temperature distribution profiles around the spot center of heat source for various powers; (d) temperature distribution profiles around the spot center of heat source for various scan speeds; (e) Molten pool sizes versus electron beam power with scan speed 1,000 mm/s; (f) molten pool size versus scan speed with beam power 600 W

both thermal and mechanical analysis, including the substrate, the solid part to be melted and the powders surrounding the solid, was constructed and meshed once. The layer-by-layer fabrication process and the layer-by-layer simulation of temperature field were realized by *MODEL CHANGE. This element birth and death technique is fully exploited here to model the AM process. When the thermal analysis is completed, a keyword *ELEMENT PROGRESSIVE ACTIVATION is used to change the full model including both solid and powder for thermal analysis to a mechanical model which only has the solid part. All the codes and files used in this paper can be found at https://github.com/XJTU-Zhou-group/ABAQUS-Codes-for-AM-Process-of-Tantalum.

3. Results of single-track selective electron beam melting process

Figure 2(a) gives the schematic of the computational model for the single-track SEBM process. A thin layer of tantalum powder with thickness 0.05 mm is spread on the top of a solid substrate with dimensions 4.2 mm × 2.1 mm × 2 mm. Also inserted in Figure 2(a) is the meshing used for simulation, and the zoom-in picture shows the local refined meshing adopted in the powder layer. In Figure 2(a), the boundary conditions for the transient heat transfer equation, equation (4), are also shown schematically.

Figure 2(b) shows the predicted morphology and sizes of the molten pool with beam power 600 W and scan speed 1,000 mm/s. Figures 2(c) and 2(d) plot the temperature distribution in the neighborhood of the moving heat source under various electron beam powers and scanning speeds, respectively. It can be seen that on the both sides of the peak temperature, there are two plateaux which correspond to melting of the tantalum powder and solidification of the liquid. The plateau on the left is more obvious. In addition, the peak temperature increases with the increase of power or decrease of scanning speed. Figure 2(e) presents the predicted sizes of molten pools under various electron beam powers, for example, 480 W, 540 W, 600 W, 660 W and 720 W, with the scanning speed 1,000 mm/s. Figure 2(f) gives the sizes of molten pools under various scanning speed with the beam power 600 W. Figures 2(e) and 2(f) indicate that, with increase of power or decrease of scanning speed, the length, width and depth of the molten pool all increase. The simulation results in Figure 2 for the SEBM process of single track lay a foundation for the following multi-track multi-layer study.

4. Results of multi-track multi-layer selective electron beam melting process

Figure 3(a) shows the schematic of the computational model of SEBM process of multi-track multi-layer. The model was constructed with a substrate 4 × 4 × 2 mm and two layers of powders each with thickness 0.05 mm. The scanning area is 2 × 2 mm. The scanning strategy is inserted in Figure 3(a). The scanning speed is 1,000 mm/s and the source power is 600 W. After the first layer is printed, there is 10 s cooling period to account for the powder deposition of the second layer and allow the temperature become uniform and reaches the preheating temperature 1,123 K. After the second layer is printed, the part

Figure 3 Computational model of multi-track multi-layer selective electron beam melting of tantalum

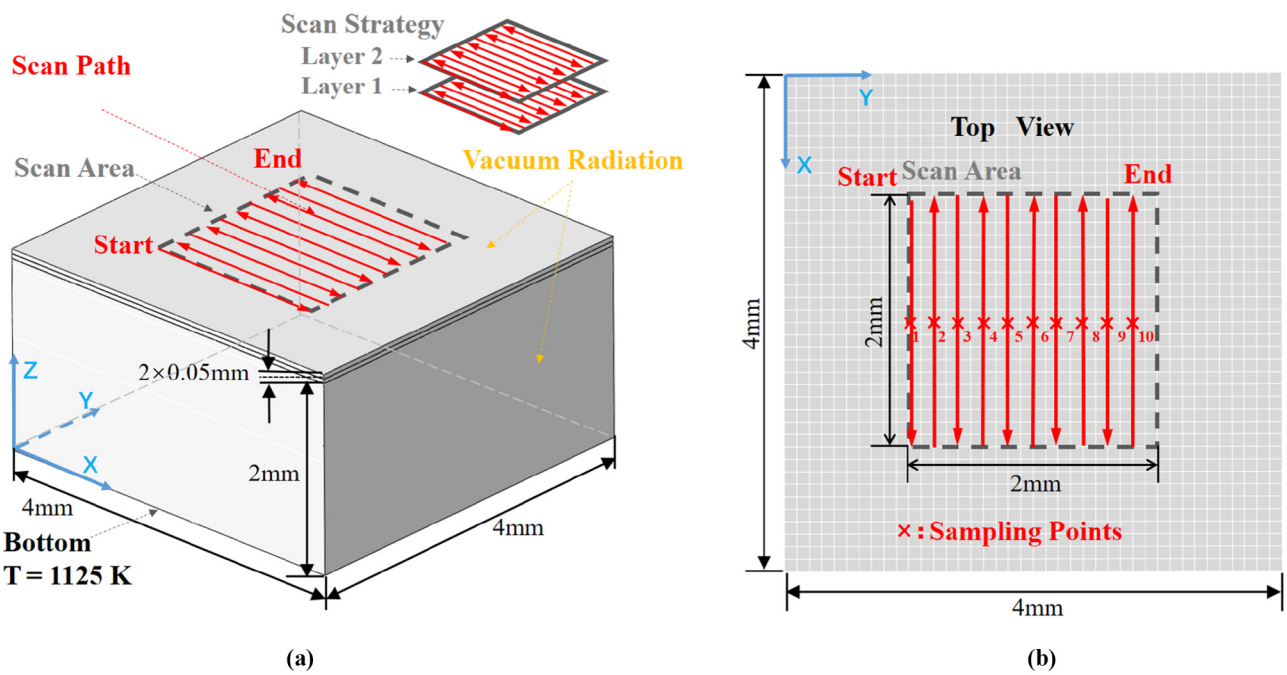

Notes: (a) Schematic of a multi-track two-layer model; (b) top view of the multiple tracks and the sampling points marked by crosses

gradually cool down to the room temperature. Note that the size of computation domain is larger than the size of scanning area, implying that the part as-fabricated is surrounded by powders. Figure 3(b) gives the top view of the multiple scanning tracks. In all, ten sample points at the midpoints of ten tracks are marked by crosses and are analyzed in details in the following discussions.

Figures 4(a) and 4(b) present the thermal history curves of the ten sampling points on the first layer and the second layer, respectively. For each sampling point, the temperature steeply increases to the maximum value once the moving heat source reaches the point and decreases gradually and levels off eventually when the heat source leaves. Because of the rapid heating, no temperature plateau is observed during the heating period. But the solidification plateau is still obvious. For a typical thermal history curve, besides the major peak, there are still two minor peaks on two sides of the major peak which indicates that the current point will be heated when the moving source pass the midpoints on the adjacent tracks.

A close look at the curves in Figure 4(a) finds that the peak temperature increase with the track number at first because of the cumulative heating effect of previous tracks. But it almost reached a steady state after the fifth track. The curves in Figure 4(b) have the similar trend as those in Figure 4(a) but reach higher peaks as compared to the corresponding track sequence in Figure 4(a).The reason can be explained as follows. In this computational model, the thickness of the substrate is only 2 mm which makes the temperature gradient and the conducive heat flux towards the substrate bottom very large. During the printing of the second layer, the substrate thickness is increased by a powder layer thickness which increases the conductive thermal resistance towards the

Figure 4 Thermal history curves of the sample points at the midpoints of all tracks on the two layers

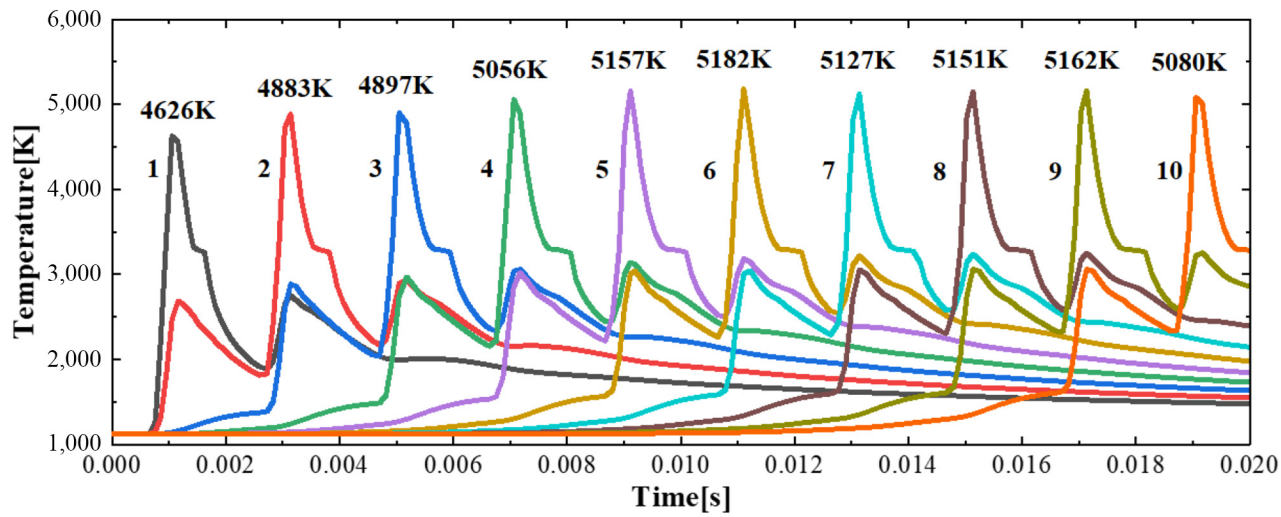

(a)

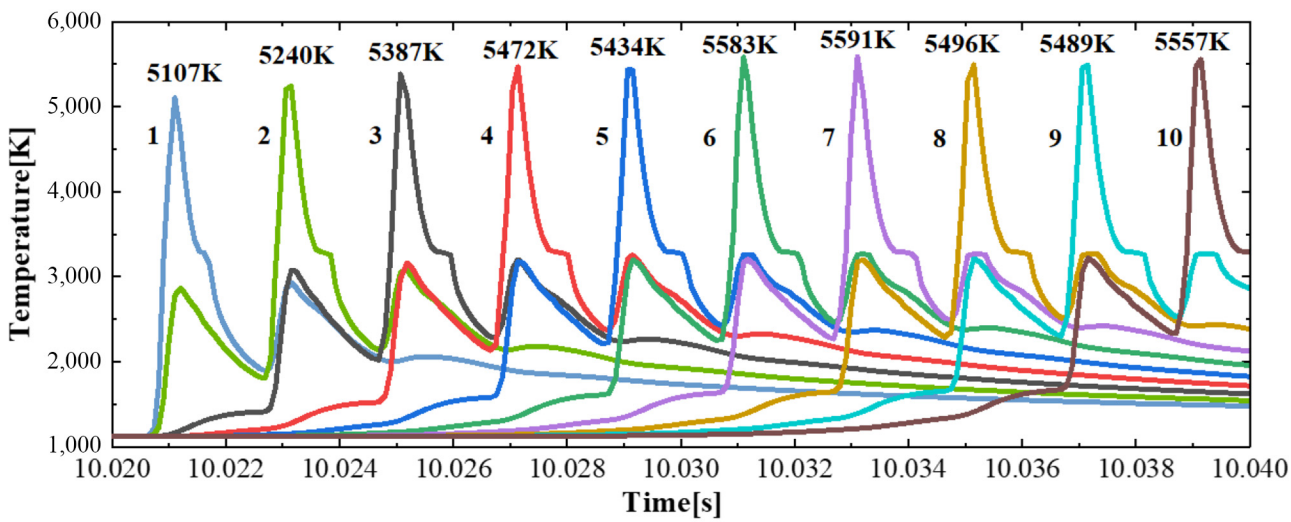

(b)

Notes: (a) The ten sampling points on the first layer; (b) the ten sampling points on the second layer

substrate bottom and results in higher peaks. For the parameters used herein, the minor peaks of the tracks 5, 6, 7, 8 and 9 for the second layer reach the melting point of tantalum (3,253 K).

Figure 5 presents the morphologies and the sizes of molten pools extracted at the ten sampling points. The sizes of the molten pool increase at first with the scanning track number and then level off after the fourth track. Accordingly, the inter-track molten pool overlapping ratio increases with the scanning track number and reaches about 100% for the last several tracks in the second layer. As shown in Figure 5(b), the molten pool depth levels-off around 0.1 mm, implying that for the conditions considered here, the two layers can fuse well along the thickness direction.

Figure 5 Predicted molten pool morphologies and sizes of multi-track multi-layer selective electron beam melting process extracted at the sampling points located at the midpoints of multiple tracks

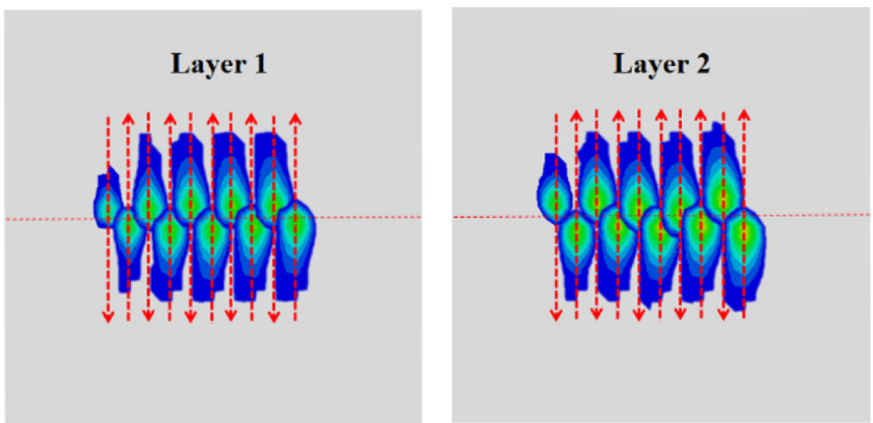

(a)

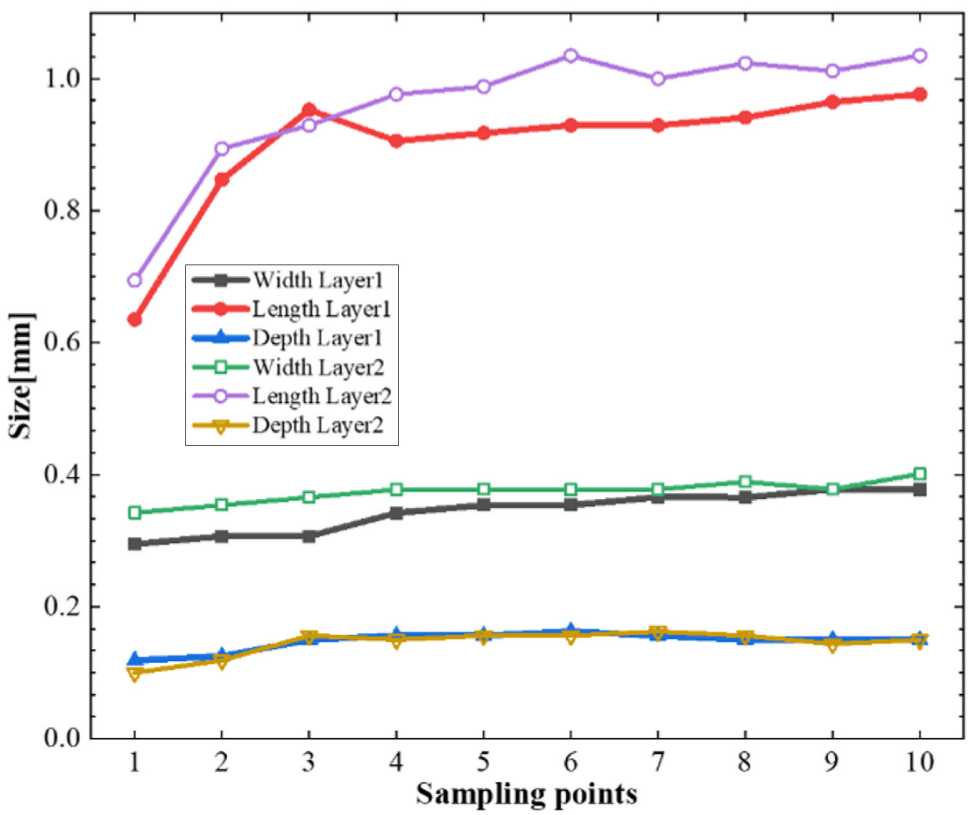

(b)

Notes: (a) Morphologies of the molten pools extracted at the sampling points located at the midpoints of multiple tracks; (b) sizes of the molten pools at the sampling points

When the transient heat transfer problem is solved and the temperature of each node is obtained, a sequential coupling scheme is adopted, and the temperature of each node is imported as thermal load to calculate the deformation and the stress distribution in the solid. An ideal elastic-plastic material law was assumed for the solid, while the powders surrounding the printed part were neglected in the stress analysis. Figure 6(a) illustrates the coordinate system and three paths along which distances are measured and stress curves are plotted. Figure 6(b) shows contours of von Mises stress, stress in *X*-direction (S11) and stress in *Y*-direction (S22). Figure 6(c) plots the residual stress profiles along three paths. It can be seen that the stresses in the region of the substrate around the part is larger than other regions. For the printed part, the center experiences larger

Figure 6 Predicted residual stress distribution when the printed part is cooled down to room temperature

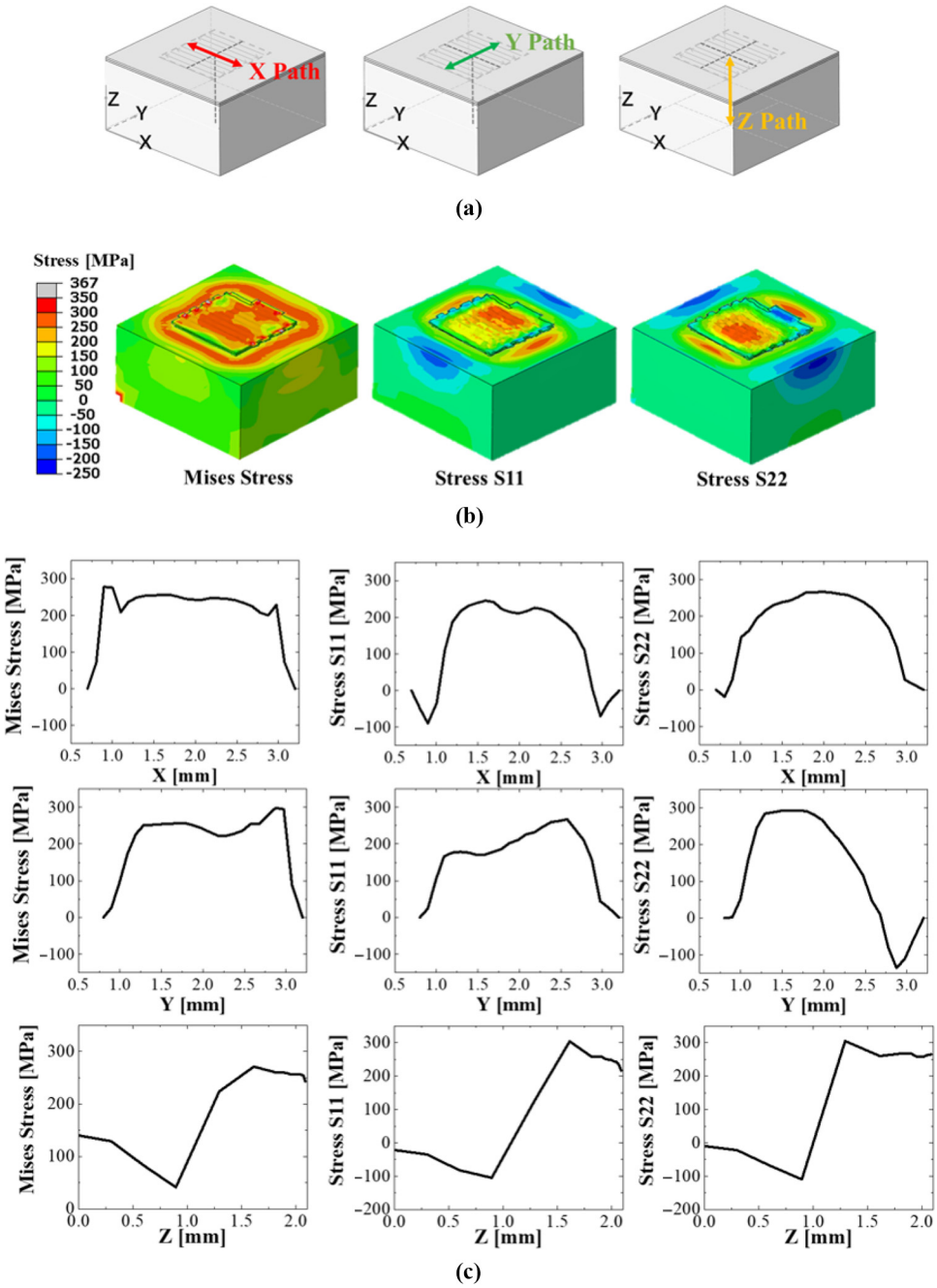

Notes: (a) Definition of *X, Y* and *Z* paths used for residual stress distribution plots; (b) contours of von Mises stress, S11 (stress component in *X*-direction) and S22 (stress component in *Y*-direction); (c) distributions of von Mises stress, S11 and S22 along different paths with beam power 600W

stresses than the edges because the edges have less constraints. As shown in Figure 6(c), the maximum stresses appear in the region nearly beneath the surface. For the residual stress components S11 and S22 in *Z*-direction, the stress is tensile in the upper part, then it decreases gradually and turns to compressive stress towards the substrate bottom. This residual stress distribution is consistent with the experimental results (Mercelis and Kruth, 2006) in the trend.

5. Modeling selective electron beam melting of a lattice structure via multi-track multi-layer fabrication

On the basis of the above-mentioned single track and multi-track multi-layer results, we now turn onto the SEBM fabrication of a cellular lattice structure. The experiments of such structures are very common, while the numerical simulation of such a complex process is very spare. Figure 7(a) gives a periodic lattice structure comprising 5 × 5 × 5 BCC unit cells with dimensions 2 mm × 2 mm × 2 mm as shown in the figure. So far, it is prohibitive to model a structure with dimensions 10 mm × 10 mm × 10 mm in Figure 7(a). Because of the periodicity of the problem, we only model a part of the structure but with proper conditions. More specifically, we make use of periodicity in *X*- and *Y*-directions and enforce periodic condition but model the real dimension in *Z*-direction. The scanning strategy of such a lattice structure should be carefully designed in a layer-wise fashion. Figure 7(b) shows the scanning strategy for a BCC unit cell. During various stages of SEBM process, the areas to be melted within different layers are different, marked by 1, 2, 3 and 4 in both iso-view and top view in Figure 7(b). In real simulation, a solid substrate was

Figure 7 Schematic of a periodic lattice structure and the scanning strategy

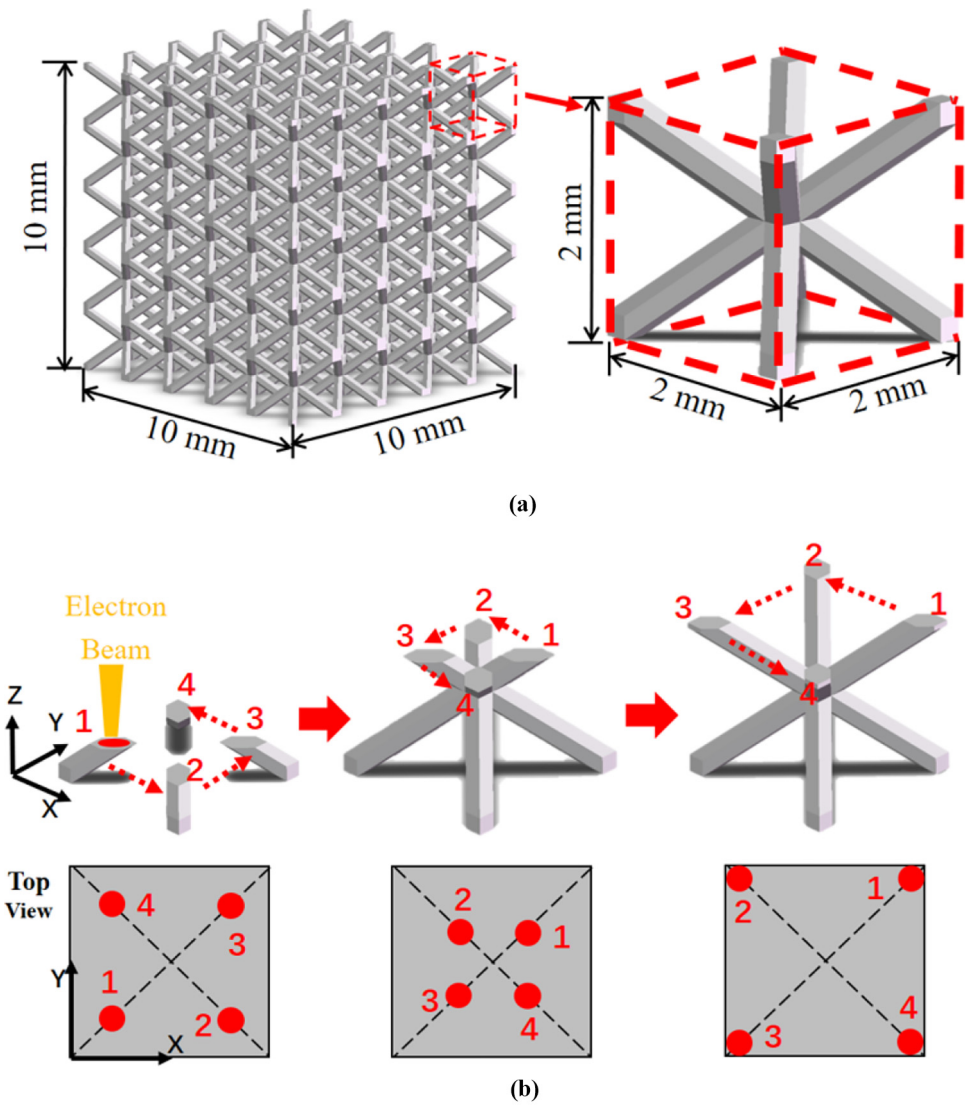

Notes: (a) A 10 × 10 × 10 mm³ lattice composed of 5 × 5 × 5 unit cells in three directions. each unit cell has dimensions 2 × 2 × 2 mm³. (b) the iso-view and the top view of the scanning strategy for the BCC unit cell

also incorporated. Figure 8(a) gives the result of thermal analysis corresponding to an instant of time, t = 107.525s, when the heating process of the tenth powder layer ends. For the purpose of better view, two contours with and without powders are given together. Figure 8(b) presents the evolution of stress during the fabrication process. Only the solid part is shown here. The instants 410.08 s, 810.16 s, 1,210.24 s, 1,610.32 s and 2,010.40 s are corresponding to the moments when the first, second, third, fourth and fifth unit cell are completed. The modeling of such a complex structure is time-consuming and a tedious task, which runs over 500 h in a supercomputing cluster with 28 CPUs. It is also an excellent example of the numerical technique developed in this paper for the multi-track multi-layer SEBM simulation.

6. Concluding remarks

Tantalum is a refractory metal with diverse applications. AM provides an alternative to the conventional fabrication technologies. Experimental efforts of AM of tantalum by using the popular powder bed-based methods, either SLM or SEBM, have been carried out, and the effectiveness and versatility of AM for tantalum have been demonstrated. No efforts, nevertheless, have been devoted to the numerical simulation of AM of tantalum, to the best knowledge of the authors.

Focusing on the SEBM AM technology, this paper presents finite element simulation of SEBM for tantalum. We firstly describe our implementation of modeling methodology and technique. We present the result for single track scanning simulation to have an understanding of the influence of scanning power and speed on the morphology of melting pool

Figure 8 Simulation of a tantalum lattice structure fabricated via selective electron beam melting with multi-track multi-layer

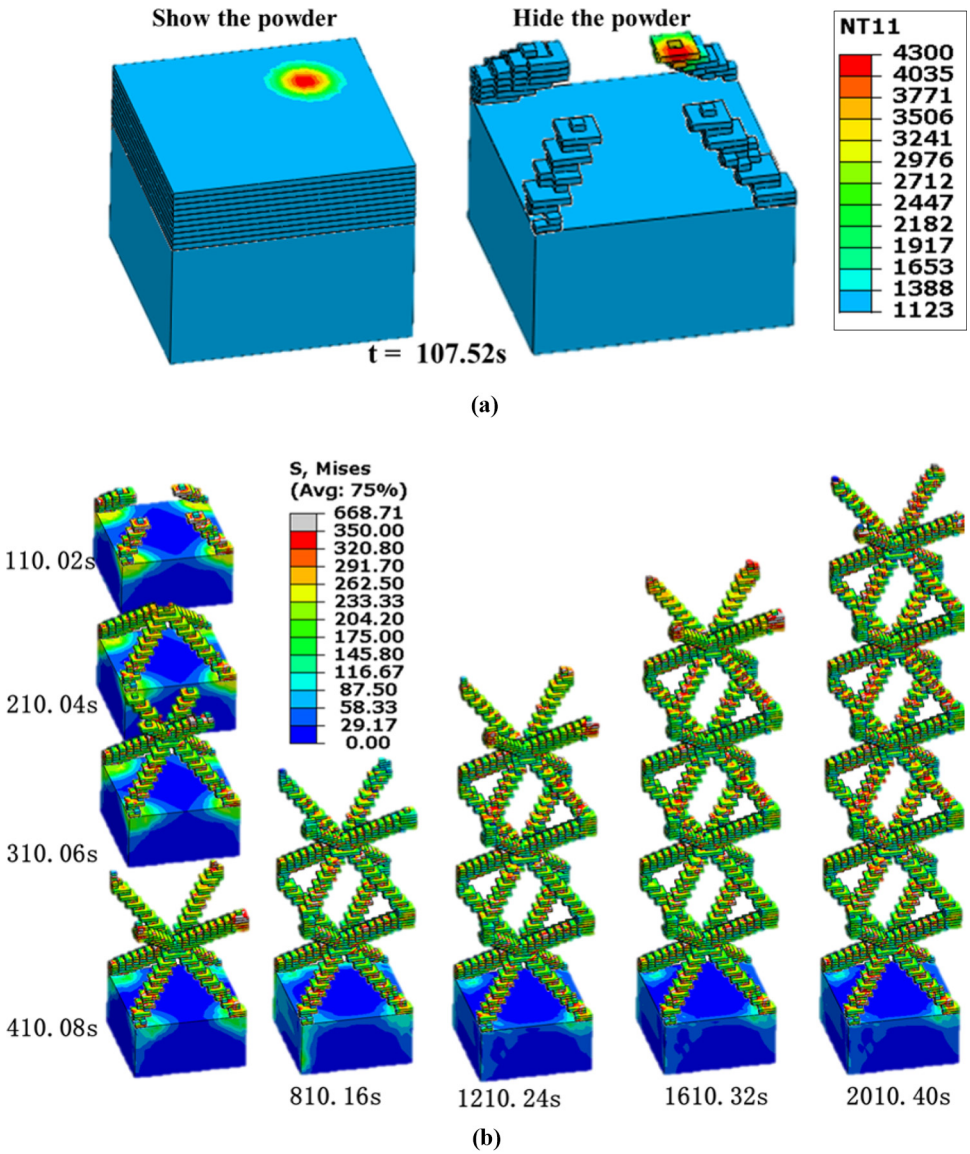

Notes: (a) Temperature distribution when ten layers were printed; (b) stress evolution during the selective electron beam melting process of a lattice structure

of tantalum. Then the study is focused on the results of multi-track multi-layer SEBM process. The key information such as inter-track molten pool overlapping ratio and inter-layer refusion state can be extracted from the obtained molten pool morphologies, which are vital for realistic failure prediction and process parameters control for real components. The predicted residual stress distributions agree with the experimental results given in literature in trend. With the help of developed simulation strategy and the powerfulness of commercial software, we finally demonstrate the SEBM manufacturing of a lattice cellular structure. The scanning path is carefully designed in a layer-wise fashion and tailored to meet the structural variations for different layers. Not only temperature distribution but also stress evolution are captured in a layer-by-layer dynamic scenario. Our efforts shed light on thermal and residual deformation control of AM products. The simulation strategy we develop here can be modified and extended straightforwardly for other AM technologies such SLM. We also publicize the data and codes for simulation, hoping to contribute the community and facilitate interaction between academia and industry.

References

An, N., Yang, G., Yang, K., Wang, J., Li, M. and Zhou, J. (2021), "Implementation of ABAQUS user subroutines and plugin for thermal analysis of powder-bed electron-beam-melting additive manufacturing process", *Materials Today Communications*, Vol. 27, p. 102307.

Beyer, C. (2014), "Strategic implications of current trends in additive manufacturing", *Journal of Manufacturing Science and Engineering*, Vol. 136 No. 6.

Cheng, B. and Chou, K. (2015), "Geometric consideration of support structures in part overhang fabrications by electron beam additive manufacturing", *Computer-Aided Design*, Vol. 69, pp. 102-111.

Cheng, B., Shrestha, S. and Chou, K. (2016), "Stress and deformation evaluations of scanning strategy effect in selective laser melting", *Additive Manufacturing*, Special Issue on Modeling & Simulation for Additive Manufacturing, Vol. 12, pp. 240-251.

Cheng, B., Price, S., Lydon, J., Cooper, K. and Chou, K. (2014), "On process temperature in powder-bed electron beam additive manufacturing: model development and validation", *Journal of Manufacturing Science and Engineering*, Vol. 136 No. 6.

Choi, G.-S., Lim, J.-W., Munirathnam, N.R., ho Kim, I. and Kim, J.-S. (2009), "Preparation of 5n grade tantalum by electron beam melting", *Journal of Alloys and Compounds*, Vol. 469 Nos 1/2, pp. 298-303.

Dallago, M., Raghavendra, S., Luchin, V., Zappini, G., Pasini, D. and Benedetti, M. (2019), "Geometric assessment of lattice materials built via selective laser melting", *Materials Today: Proceedings*, Vol. 7, pp. 353-361.

Denlinger, E.R., Gouge, M., Irwin, J. and Michaleris, P. (2017), "Thermomechanical model development and in situ experimental validation of the laser powder-bed fusion process", *Additive Manufacturing*, Vol. 16, pp. 73-80.

Dong, F., Chen, Y., Bai, Z., Wang, H. and Jiang, L. (2019), "Microstructures and mechanical properties of tungsten-tantalum alloys consolidated by electron beam melting, hot pressing and spark plasma sintering", *IOP Conference Series: Materials Science and Engineering*, Vol. 558 No. 1, p. 12008 (6pp).

Duan, S., Xi, L., Wen, W. and Fang, D. (2020), "Mechanical performance of topology-optimized 3d lattice materials manufactured via selective laser sintering", *Composite Structures*, Vol. 238, p. 111985.

Dumas, M., Terriault, P. and Brailovski, V. (2017), "Modelling and characterization of a porosity graded lattice structure for additively manufactured biomaterials", *Materials & Design*, Vol. 121, pp. 383-392.

Evans, A.G., Hutchinson, J.W., Fleck, N.A., Ashby, M. and Wadley, H. (2001), "The topological design of multifunctional cellular metals", *Progress in Materials Science*, Vol. 46 Nos 3/4, pp. 309-327.

Fachinotti, V.D., Anca, A.A. and Cardona, A. (2011), "Analytical solutions of the thermal field induced by moving double-ellipsoidal and double-elliptical heat sources in a semi-infinite body", *International Journal for Numerical Methods in Biomedical Engineering*, Vol. 27 No. 4, pp. 595-607.

Galati, M. and Iuliano, L. (2018), "A literature review of powder-based electron beam melting focusing on numerical simulations", *Additive Manufacturing*, Vol. 19, pp. 1-20.

Galati, M., Iuliano, L., Salmi, A. and Atzeni, E. (2017), "Modelling energy source and powder properties for the development of a thermal FE model of the EBM additive manufacturing process", *Additive Manufacturing*, Vol. 14, pp. 49-59.

Goldak, J. (1985), "A double ellipsoid finite element model for welding heat sources", IIW Doc. No. 212.

Gorguluarslan, R.M., Gandhi, U.N., Mandapati, R. and Choi, S.-K. (2016), "Design and fabrication of periodic lattice-based cellular structures", *Computer-Aided Design and Applications*, Vol. 13 No. 1, pp. 50-62.

Helou, M. and Kara, S. (2018), "Design, analysis and manufacturing of lattice structures: an overview", *International Journal of Computer Integrated Manufacturing*, Vol. 31 No. 3, pp. 243-261.

Helou, M., Vongbunyong, S. and Kara, S. (2016), "Finite element analysis and validation of cellular structures", *Procedia CIRP*, Vol. 50, pp. 94-99.

Herzog, D., Seyda, V., Wycisk, E. and Emmelmann, C. (2016), "Additive manufacturing of metals", *Acta Materialia*, Vol. 117, pp. 371-392.

Leary, M., Mazur, M., Elambasseril, J., McMillan, M., Chirent, T., Sun, Y., Qian, M., Easton, M. and Brandt, M. (2016), "Selective laser melting (slm) of alsi12mg lattice structures", *Materials & Design*, Vol. 98, pp. 344-357.

Li, C., Fu, C., Guo, Y. and Fang, F. (2016), "A multiscale modeling approach for fast prediction of part distortion in selective laser melting", *Journal of Materials Processing Technology*, Vol. 229, pp. 703-712.

Li, C., Liu, J., Fang, X. and Guo, Y. (2017), "Efficient predictive model of part distortion and residual stress in selective laser melting", *Additive Manufacturing*, Vol. 17, pp. 157-168.

Li, S., Murr, L.E., Cheng, X., Zhang, Z., Hao, Y., Yang, R., Medina, F. and Wicker, R. (2012), "Compression fatigue

behavior of ti–6al–4v mesh arrays fabricated by electron beam melting", *Acta Materialia*, Vol. 60 No. 3, pp. 793-802.

Li, Y., Zhou, K., Tan, P., Tor, S.B., Chua, C.K. and Leong, K.F. (2018), "Modeling temperature and residual stress fields in selective laser melting", *International Journal of Mechanical Sciences*, Vol. 136, pp. 24-35.

Lu, T., He, D., Chen, C., Zhao, C., Fang, D. and Wang, X. (2006), "The multi-functionality of ultra-light porous metals and their applications", *Advances in Mechanics*, Vol. 36 No. 4, pp. 517-535.

Mercelis, P. and Kruth, J.-P. (2006), "Residual stresses in selective laser sintering and selective laser melting", *Rapid Prototyping Journal*, Vol. 12 No. 5.

Pan, C., Han, Y. and Lu, J. (2020), "Design and optimization of lattice structures: a review", *Applied Sciences*, Vol. 10 No. 18, p. 6374.

Parthasarathy, J., Starly, B., Raman, S. and Christensen, A. (2010), "Mechanical evaluation of porous titanium (ti6al4v) structures with electron beam melting (EBM)", *Journal of the Mechanical Behavior of Biomedical Materials*, Vol. 3 No. 3, pp. 249-259.

Powell, R.W., Ho, C.Y. and Liley, P.E. (1968), *Thermal Conductivity of Selected Materials*, US Department of Commerce, Washing, DC.

Queheillalt, D.T. and Wadley, H.N. (2005), "Cellular metal lattices with hollow trusses", *Acta Materialia*, Vol. 53 No. 2, pp. 303-313.

Rahmani, R., Antonov, M., Kollo, L., Holovenko, Y. and Prashanth, K.G. (2019), "Mechanical behavior of ti6al4v scaffolds filled with casio3 for implant applications", *Applied Sciences*, Vol. 9 No. 18, p. 3844.

Shabalin, I.L. (2014), *Ultra-high temperature materials – Carbon (Graphene/Graphite) and Refractory Metals*, Springer, W, Re, Os, Ta, Mo, Nb, Ir (Front Matter), Vol. 1.

Shen, N. and Chou, K. (2012), "Thermal modeling of electron beam additive manufacturing process: powder sintering effects", *ASME 2012 International Manufacturing Science and Engineering Conference of International Manufacturing Science and Engineering Conference*.

Sing, S.L., Wiria, F.E. and Yeong, W.Y. (2018), "Selective laser melting of titanium alloy with 50. wt% tantalum: effect of laser process parameters on part quality", *International Journal of Refractory Metals and Hard Materials*, Vol. 77, pp. 120-127.

Sing, S.L., Wiria, F.E. and Yeong, W.Y. (2018), "Selective laser melting of lattice structures: a statistical approach to manufacturability and mechanical behavior", *Robotics and Computer-Integrated Manufacturing*, Vol. 49, pp. 170-180.

Škoro, G.P., Bennett, J.R.J. and Edgecock, T.R. (2011), "Dynamic young's moduli of tungsten and tantalum at high temperature and stress", *Journal of Nuclear Materials*, Vol. 409 No. 1, pp. 40-46.

Škoro, G., Bennett, J., Edgecock, T. and Booth, C. (2012), "Yield strength of molybdenum, tantalum and tungsten at high strain rates and very high temperatures", *Journal of Nuclear Materials*, Vol. 426 Nos 1/3, pp. 45-51.

Soro, N., Attar, H., Brodie, E., Veidt, M., Molotnikov, A. and Dargusch, M.S. (2019), "Evaluation of the mechanical compatibility of additively manufactured porous ti–25ta alloy for load-bearing implant applications", *Journal of the Mechanical Behavior of Biomedical Materials*, Vol. 97, pp. 149-158.

Suard, M., Martin, G., Lhuissier, P., Dendievel, R., Vignat, F., Blandin, J.-J. and Villeneuve, F. (2015), "Mechanical equivalent diameter of single struts for the stiffness prediction of lattice structures produced by electron beam melting", *Additive Manufacturing*, Vol. 8, pp. 124-131.

Takezawa, A., Yonekura, K., Koizumi, Y., Zhang, X. and Kitamura, M. (2018), "Isotropic ti–6al–4v lattice via topology optimization and electron-beam melting", *Additive Manufacturing*, Vol. 22, pp. 634-642.

Tancogne-Dejean, T., Diamantopoulou, M., Gorji, M.B., Bonatti, C. and Mohr, D. (2018), "3d plate-lattices: an emerging class of low-density metamaterial exhibiting optimal isotropic stiffness", *Advanced Materials*, Vol. 30 No. 45, p. 1803334.

Tantalum (2021), available at: www.plansee.com/en/materials/tantalum.html (accessed 6 March 2021).

Thijs, L., Sistiaga, M.L.M., Wauthle, R., Xie, Q., Kruth, J.-P. and Humbeeck, J.V. (2013), "Strong morphological and crystallographic texture and resulting yield strength anisotropy in selective laser melted tantalum", *Acta Materialia*, Vol. 61 No. 12, pp. 4657-4668.

Tolochko, N.K., Arshinov, M.K., Gusarov, A.V., Titov, V.I., Laoui, T. and Froyen, L. (2003), "Mechanisms of selective laser sintering and heat transfer in ti powder", *Rapid Prototyping Journal*, Vol. 9 No. 5, pp. 314-326.

Vasiliev, V.V., Barynin, V.A. and Razin, A.F. (2012), "Anisogrid composite lattice structures – development and aerospace applications", *Composite Structures*, Vol. 94 No. 3, pp. 1117-1127.

Wadley, H.N., Fleck, N.A. and Evans, A.G. (2003), "Fabrication and structural performance of periodic cellular metal sandwich structures", *Composites Science and Technology*, Vol. 63 No. 16, pp. 2331-2343.

Wang, J., Evans, A.G., Dharmasena, K. and Wadley, H.G. (2003), "On the performance of truss panels with kagome cores", *International Journal of Solids and Structures*, Vol. 40 No. 25, pp. 6981-6988.

Warmuth, F., Osmanlic, F., Adler, L., Lodes, M.A. and Körner, C. (2016), "Fabrication and characterisation of a fully auxetic 3d lattice structure via selective electron beam melting", *Smart Materials and Structures*, Vol. 26 No. 2, p. 25013.

Wong, K.V. and Hernandez, A. (2012), "A review of additive manufacturing", *International Scholarly Research Notices*, Vol. 2012.

Xiao, L., Song, W., Hu, M. and Li, P. (2019), "Compressive properties and micro-structural characteristics of ti–6al–4v fabricated by electron beam melting and selective laser melting", *Materials Science and Engineering: A*, Vol. 764, p. 138204.

Xiao, Z., Yang, Y., Xiao, R., Bai, Y., Song, C. and Wang, D. (2018), "Evaluation of topology-optimized lattice structures manufactured via selective laser melting", *Materials & Design*, Vol. 143, pp. 27-37.

Yan, W., Qian, Y., Ge, W., Lin, S., Liu, W.K., Lin, F. and Wagner, G.J. (2018), "Meso-scale modeling of multiple-layer fabrication process in selective electron beam melting: inter-layer/track voids formation", *Materials & Design*, Vol. 141, pp. 210-219.

Yuan, S., Shen, F., Bai, J., Chua, C.K., Wei, J. and Zhou, K. (2017), "3d soft auxetic lattice structures fabricated by selective laser sintering: TPU powder evaluation and process optimization", *Materials & Design*, Vol. 120, pp. 317-327.

Zäh, M.F. and Lutzmann, S. (2010), "Modelling and simulation of electron beam melting", *Production Engineering*, Vol. 4 No. 1, pp. 15-23.

Zhou, L., Yuan, T., Li, R., Tang, J., Wang, G. and Guo, K. (2017), "Selective laser melting of pure tantalum: densification, microstructure and mechanical behaviors", *Materials Science and Engineering: A*, Vol. 707, pp. 443-451.

Corresponding author

Meie Li can be contacted at: limeie@mail.xjtu.edu.cn